K. Rama Mohan
Assistant Professor.
VNR Vignana Jyothi
Institute of Engineering and Technology,
Batchpally, Hyderabad,
Andhra Pradesh,
India

C. M. Vara Parasad
Principal.
Sri Venkateswara
Engineering College, Suryapet,
Nalgonda (Dt.),
Andhra Pradesh,
India

M. V. S. Murali Krishna
Senior Lecturer.
Mechanical Engineering Department,
Chaitanya Bharati Institute of Technology,
Gandipet, Hyderabad,
Andhra Pradesh,
India

Performance of a Low Heat Rejection Diesel Engine With Air Gap Insulated Piston

A threaded air gap insulated piston provided effective insulation without causing sealing problems. The performance of the diesel engine with the air gap insulated piston was obtained with different piston crown materials, at differing magnitudes of air gap with varying injection timings. The engine using Nimonic for the piston crown with an air gap of 3 mm at an injection timing of 29.5° bTDC reduced the BSFC by 12 percent at part loads and 4 percent at full load. The performance in terms of P-θ and T-θ was predicted employing a zero dimensional multizone combustion model, and the model results have been validated with measured pressures and the exhaust gas temperatures. More appropriate piston surface temperatures were employed in Annand's equation to improve the computer predictions using finite element modeling of the piston. The measured temperatures of air in the air gap using an L-link mechanism provided excellent validation for the finite element prediction of isotherms in the piston.

Introduction

The second law requirement of Thermodynamics necessitates the inevitable heat loss to the coolant to realise work output. Any saving in this part of the energy distribution would either increase the energy lost through exhaust gases or increase the power output. Considerable efforts are under way to reduce heat loss to the coolant by various researchers. However, the results are a little confusing as to whether the insulation would improve or deteriorate thermal efficiency. The two approaches that are being pursued to decrease heat rejection are (1) ceramic coating and (2) air gap insulation. Both these methods are still having problems. Ceramic coatings are found to be peeling off over a period of operation. There are serious problems of leakage of gases in the case of air gap insulation.

Krishnan et al. (1980) and Wade et al. (1984) observed an improvement in thermal efficiency with ceramic coated components. While Woschni et al. (1987) and Cole et al. (1985) reported reduction in BSFC with an air gap insulated piston at part loads, Woschni found deterioration of engine performance and Cole observed no change in fuel economy at full load. However Cheng et al. (1989) reported that the BSFC increased when chamber walls were insulated with ceramic coatings and Alkidas et al. (1987) found deterioration of engine performance with air gap insulated piston. Though Cole et al. and Parker et al. (1987) observed effective insulation provided by an air gap, the bolted design employed by them could not provide complete sealing of air in the air gap. While Seigla et al. (1989) and Miyairi et al. (1988) found deterioration of engine performance with retarded injection timings, Dhinagar et al. (1989) claimed improved performance with retarded injection timing in low heat rejection (LHR) engines.

A two zone combustion model was used by Miyairi (1988) and a computer simulation model was used by Rafiqul Islam et al. (1991) for predicting the performance of the ceramic coated direct injection (DI) diesel engines.

A study of the existing literature on LHR engines thus reveals inconclusive results. There is not only a need to develop a satisfactory technique of joining the crown with the piston body, achieving complete and durable sealing of the air gap, but also to adjust the injection timing as the combustion phenomenon in LHR engines gets modified. No systematic study has been reported on the use of different crown materials with varying magnitudes of air gap for an air gap insulated piston. The performance of the engine with an air gap insulated piston employing different crown materials with varying magnitudes of the air gap is reported in this paper. The paper also attempts to develop a multizone model with more appropriate input for more precise prediction of performance of LHR engines.

Experimental Program

As an attempt to insulate the combustion chamber, a threaded design of air gap insulated piston was employed in a single cylinder direct injection diesel engine. The details of the air gap provided in the piston are shown in the Fig. 1.

This design could provide perfect sealing of air in the air gap. Figure 2 shows the experimental setup employed. The test engine (1) which is a constant speed engine has an aluminum alloy piston with a bore of 80 mm and a stroke of 110 mm. The rated output of the engine was 3.68 kW at the rated speed of 1500 rpm. The compression ratio 16:1 and the manufacturer's recommended injection timing and injection pressure are 27° bTDC and 195 bars, respectively. The fuel injector has 3 holes of size 0.25 mm. The combustion chamber consists of direct injection type with no special arrangement for swirling motion of air. The naturally aspirated engine was provided with water cooling system in which the outlet water temperature was maintained at 60°C by adjusting the water flow rate. The engine oil was provided with a pressure feed system and no temperature control was provided for measuring oil temperature. The engine is coupled to a hydraulic dynamometer (2). Air and fuel consumption were measured using air flow meter (3) and fuel measuring pipette (4). The outlet temperature of water and the exhaust gas temperatures were observed using a gas thermometer (5) and an iron-iron constantan thermocouple connected to temperature indicator (6). The mass flow rate of cooling water is measured using a measuring tank (7). The piston temperatures are noted using an iron-iron constantan ther-

Contributed by the Internal Combustion Engine Division (ICE) of THE AMERICAN SOCIETY OF MECHANICAL ENGINEERS for publication in the ASME JOURNAL OF ENGINEERING FOR GAS TURBINES AND POWER.
Manuscript received by the ICE February 10, 1997; final revision received by the ASME Headquarters March 3, 1999. Associate Technical Editor: D. Assanis.

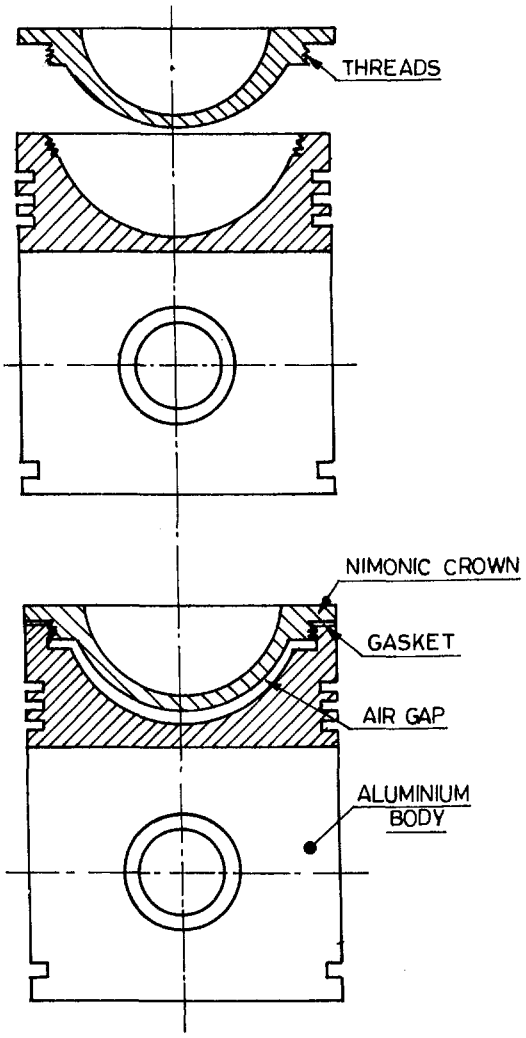

Fig. 1 Details of air gap insulated piston

mocouple (8) connected through an L-link mechanism (9) millivoltmeter (10). The pressure crank angle diagrams were obtained at full load operation of the engine with each piston configuration

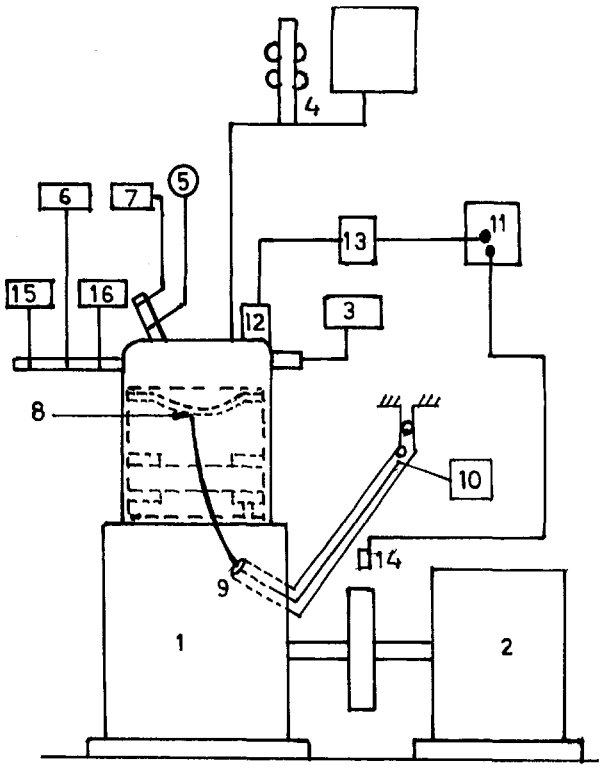

Fig. 2 Experimental set-up

using a double beam oscilloscope (11), Kistler piezo electric pressure transducer (12), charge amplifier (13), and a magnetic pickup (14). The smoke levels of the engine were noted using a Nisalco smoke meter (15). Exhaust pollutants CO and NOx were measured using a sophisticated microprocessor based TMT-36 stack analyser (16). With each configuration of air gap insulated piston load tests were carried out from which performance data like brake specific fuel consumption (BSFC), exhaust gas temperature (EGT), coolant load and volumetric efficiency were calculated for different brake mean effective pressures (BMEP). Based on the pressure crank angle diagrams, combustion parameters like peak pressure (PP), time of occurrence of peak pressure (TOPP), maximum rate of pressure rise (MRPR), and average rate of pressure rise (ARPR) were evaluated.

Nomenclature

a, b, c = constants in Annand's equation
aTDC = after top dead center
A = area
bTDC = before top dead center
B = Spalding number
C_p, C_v = specific heat at constant pressure or volume
D = binary diffusion coefficient
D_1 = cylinder bore
D_{32} = Sauter mean diameter
F_w = validation constant
h = enthalpy
HSU = Hartridge smoke units
IT = injection timing
k = thermal conductivity
M = mass
N = number of droplets
phi = equivalence ratio
ppm = parts per million
P = pressure
Q = heat transfer
dQ = net Heat Release
r = radius
R = universal gas constant
Re = Reynolds number
t = time
T = temperature
v = velocity
V = volume
X = spray penetration length
Y = mass fraction of a chemical species
ρ = density
θ = crank angle
τ = ignition delay

Subscripts

a = air
ai = after injection
b = burnt
c = combustion
e = entrainment
f = fuel
inj = injection
i, j = indexes for the elements in axial and radial directions
s = surface of a droplet
NS = index for chemical species
n = net
st = stoichiometric
ae = air entrainment
l = liquid
v = vapour
w = wall
p = piston
h = cylinder head

Table 1 Thermo-physical properties of different crown materials employed

Property	Material			
	Al-Alloy	Nimonic	SS	MS
Tehrmal Conductivity (W/m-K)	175	12	36.3	53.6
Density (Kg/m^3)	2700	8000	77.53	78.33
Modulus of Elasticity (Pascal) x 10^{-11}	0.703	1.86	1.9	2.01
Specific heat (kJ/kg-K)	0.921	0.461	0.486	0.465
Poission's ratio	0.3	0.30	0.305	0.292

Different Configurations of Air Gap Insulated Piston

The experiments were carried out with various crown materials Nimonic, stainless steel (SS) (Austenitic) and mild steel (MS). With each crown material the magnitudes of different air gaps employed were 1, 2, 3, and 3.8 mm. The composition of the Nimonic material used is 3 percent Fe, 77.1 percent Ni, 0.3 percent Ti, 0.1 percent C and 19.5 percent Cr. The thermo-physical properties of the different crown materials employed are given in Table 1.

Experiments With Different Injection Timings

As the combustion system was modified for the low heat rejection concept, performance tests were also conducted with various advanced injection timings which included 25, 27, 28.5, 29, and 29.5° bTDC. The injection timing for the conventional engine was 27° bTDC. The injection timing was varied by employing suitable copper shims between the pump body and the engine frame.

Results and Discussions

(A) Performance Parameters. The performance tests were carried out on the diesel engine with a conventional piston and with different configurations of air gap insulated piston. Among various materials tested like Nimonic, mild steel, and stainless steel for the piston cap, Nimonic is found to provide better performance on the basis of lowest magnitude of BSFC. A 3 mm air gap is found to be optimum among various air gaps tested. Figure 3 shows the variation of BSFC with BMEP for the conventional piston at an injection timing of 27° bTDC and the piston with Nimonic crown with 3 mm air gap at 27 and 29.5° bTDC. The air gap insulated piston with Nimonic crown with an injection timing of 27° bTDC gave lower BSFC upto 80 percent of full load in comparison with the conventional piston. Beyond 80 percent of full load BSFC for the insulated piston increased over and above that of the conventional piston. The reason for the deterioration of the engine performance at higher loads might be due to the friction and increased diffusion combustion resulting from reduced ignition delay due to higher temperatures. Increased radaition heat losses might have also contributed to the deterioration. The draw back of higher BSFC at full load with air gap piston disappeared with advanced injection timing of 29.5° bTDC. As the injection timing was advanced BSFC reduced further at all the loads. This shows that a significant part of the retained heat is directly converted to piston work rather than being merely available in the exhaust stream, from which it would be recoverable giving much lower BSFC. The air gap insulated piston engine with Nimonic crown and 3 mm air gap at an injection timing of 29.5° bTDC decreased the BSFC by 4 percent at full load and 12 percent at part loads in comparison with the conventional engine operating with the manufacturer's recommended injection timing of 27° bTDC. It can be observed that the magnitudes of BSFC are a little high on all versions of the engine as the test engine was an old engine which has run for a large number of hours. However, in view of this, the comparison

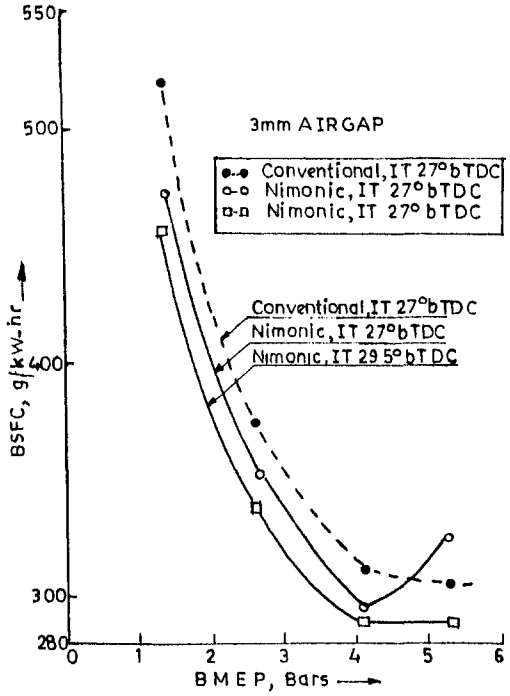

Fig. 3 Variation of BSFC with BMEP for conventional piston at 27° bTDC and insulated piston with Nimonic crow at 27° bTDC and 29.5° bTDC

was not done on ISFC basis. It can also be noted that the magnitudes of BSFC can also be affected by the oil temperature variation. As the oil temperatures were not measured, this aspect is not taken into consideration while reporting BSFC values.

Figure 4 shows the variation of BSFC with injection timing, which agreed with the trends reported by Miyairi (1989) and Seigla (1989).

Figures 5 and 6 present the variation of EGT and coolant load with BMEP for the conventional piston at 27° bTDC and insulated piston with Nimonic crown at 27° and 29.5° bTDC. EGT for the insulated piston at 27° bTDC increased throughout the load range. But when the injection timing was maintained at 29.5° bTDC, EGT for the insulated piston reduced in comparison to the operation at 27° bTDC on the same insulated piston confirming the conversion of retained heat to the piston work.

Coolant load for the insulated piston at 27° bTDC reduced up to a load of 80 percent of full load in comparison with that for conventional piston.

Beyond this load, the insulated piston with injection timing of 27° bTDC showed increase in coolant load in comparison with that

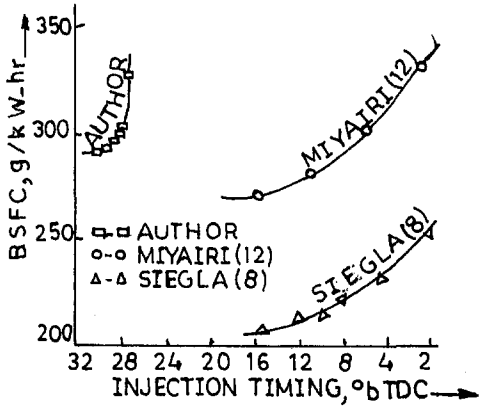

Fig. 4 Variation of BSFC with injection timings for the insulated piston engine

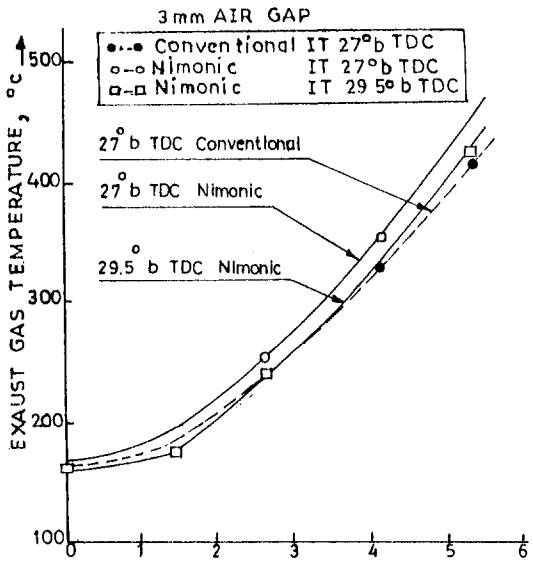

Fig. 5 Variation of EGT with BMEP for conventional piston at 27° bTDC and insulated piston with Nimonic crow at 27° bTDC and 29.5° bTDC

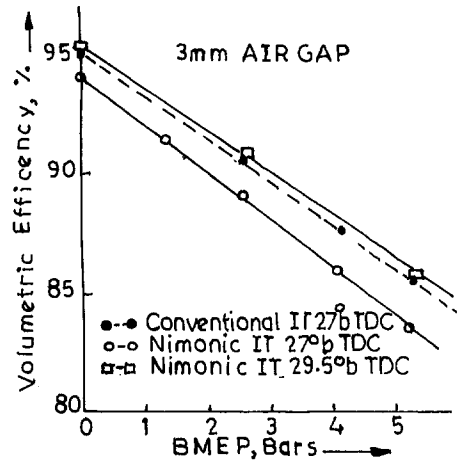

Fig. 7 Variation of volumetric efficiency with BMEP for conventional piston at 27° bTDC and insulated piston with Nimonic crow at 27° bTDC and 29.5° bTDC

for conventional piston. This is because incylinder heat rejection at full load is primarily due to unburnt fuel concentration near the combustion chamber walls. This trend has also been reported by Wallace et al. (1984). The air fuel ratio got reduced to a reasonably low value at this load confirming the above trend. However, when the injection timing was maintained at 29.5° bTDC the coolant load for the same insulated piston decreased at all loads in comparison with conventional piston. This is because at advanced injection timing, the part of retained energy gets converted into useful work giving lower EGT values. This aspect is further confirmed in the observation of EGT and BSFC magnitudes. However, when heat rejection calculations of coolant load are made, the heat lost to lubricant should also be considered. As in the present investigation the lubricant heat loss is not considered, this aspect is not depicted in the coolant load calculations.

Figure 7 presents the variation of volumetric efficiency with BMEP for the conventional piston at 27° bTDC and the piston with Nimonic crown at 27° and 29.5° bTDC.

While the volumetric efficiency for the insulated piston at 27° bTDC reduced in comparison to the conventional piston, it increased when the injection timing was maintained at 29.5° bTDC. With increase in insulation, the volumetric efficiency naturally decreases because of heating effect of incoming air. However, with advanced injection timing the gas temperature gets reduced leading to an increase in volumetric efficiency.

(B) Pollution Parameters. Figure 8 presents the variation of smoke density with BMEP for the conventional piston at 27° bTDC and insulated piston with Nimonic crown at 27 and 29.5° bTDC. Though smoke densities were lower up to a load of 80 percent of full load, at loads higher than this, the smoke density increased over and above that of conventional piston. This increase is due to decrease in volumetric efficiency and air fuel ratio. This is also due to fuel cracking at higher temperatures leading to increased smoke density.

With the injection timing of 29.5° bTDC for the insulated piston the smoke density reduced at all loads.

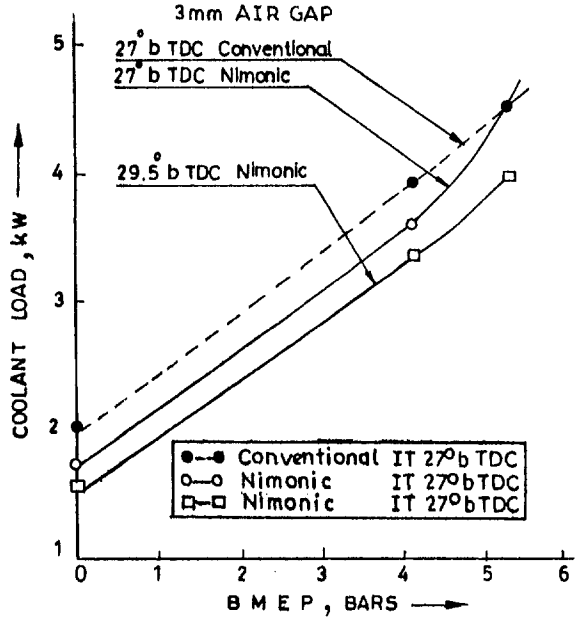

Fig. 6 Variation of coolant load with BMEP for conventional piston at 27° bTDC and insulated piston with Nimonic crow at 27° bTDC and 29.5° bTDC

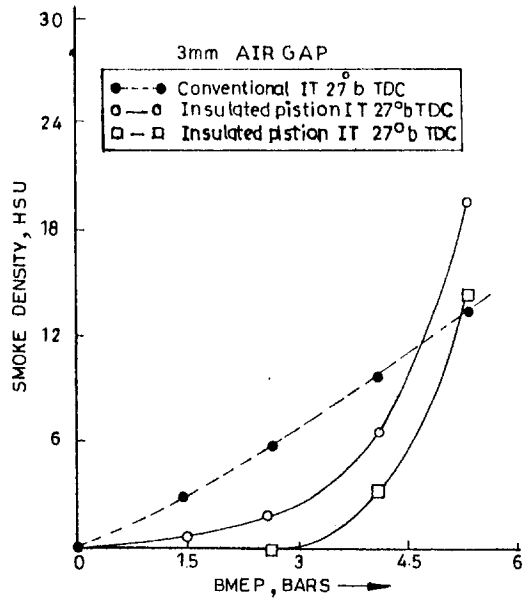

Fig. 8 Variation of smoke density with BMEP for conventional piston at 27° bTDC and insulated piston with Nimonic crow at 27° bTDC and 29.5° bTDC

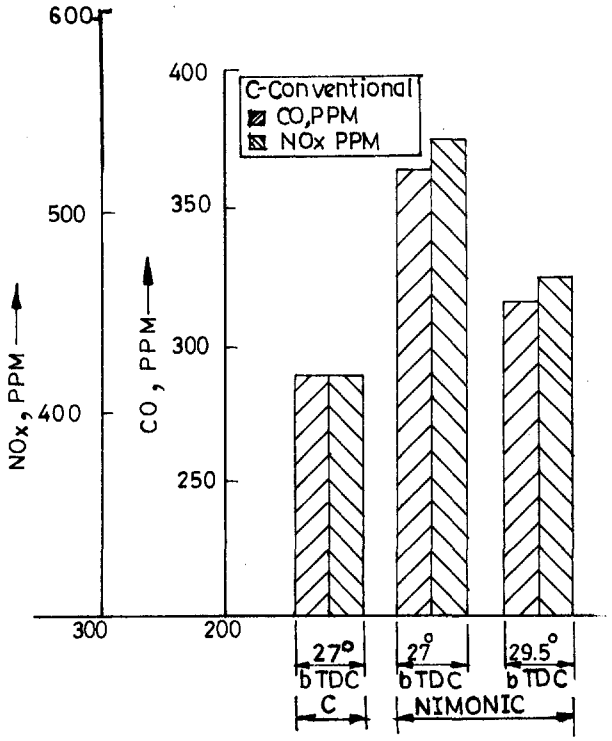

Fig. 9 Bar graphs of NOx and CO for conventional piston at 27° bTDC and insulated piston with Nimonic crown 27° bTDC and 29.5° bTDC

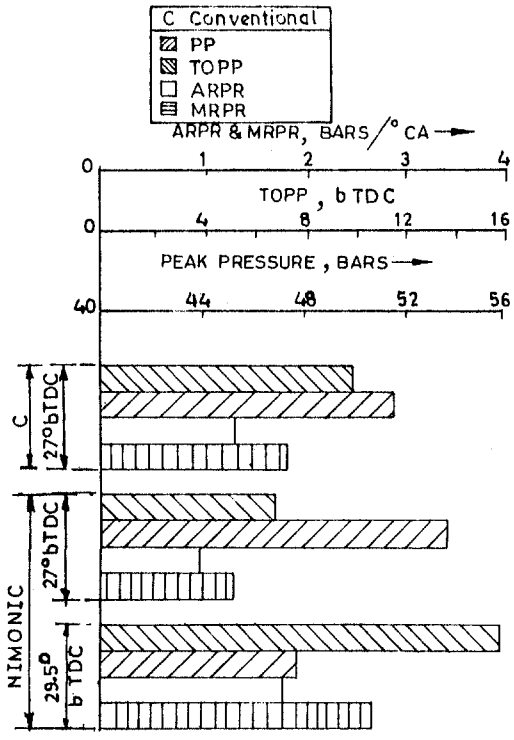

Fig. 11 Bar graphs of combustion parameters for conventional piston at 27° bTDC and insulated piston at 27° bTDC and 29.5° bTDC

Figure 9 gives the bar charts of the magnitudes of CO and NOx at full load operation of the engine. As expected, NOx increased for an insulated piston due to elevated temperatures. With advanced injection timing of 29.5° bTDC, NOx levels decreased with same insulated piston in comparison with the operation at 27° bTDC. This is because of reduction in gas temperature due to the increase in volumetric efficiency at advanced injection timings. The figure also presents data on CO emissions. One can expect that CO is not a significant pollutant in diesel engines. However, in insulated engines, many researchers presented CO emissions. Hence, the authors also measured and presented CO emissions observed in insulated engines. CO levels increased with the insulated piston because of dissosiation of CO_2 at higher temperatures.

Once again CO levels decreased with injection timing of 29.5° bTDC in comparison with the 27° bTDC on the same insulated engine. As explained earlier this is also because of reduced gas temperatures which reduced the cracking of CO_2.

(C) Combustion Parameters. Figure 10 gives the pressure-crank angle diagrams obtained from the photographs taken from the oscilloscope screen for three configurations of the conventional piston with an injection timing of 27° bTDC and insulated piston at 27 and 29.5° bTDC. Figure 11 shows the combustion parameters for the conventional piston at 27° bTDC and insulated piston with Nimonic crown at 27 and 29.5° bTDC at full load.

The peak pressures and rates of pressure rise at an injection timing of 27° bTDC were observed to be lower with the insulated piston in comparison with the conventional piston whereas peak pressures were found to occur much later from TDC. This is because the insulated piston exhibits higher temperatures of chamber walls leading to continuation of combustion, giving peak pressure away from TDC. However, this phenomenon is nullified with an injection timing of 29.5° bTDC on the same insulated piston because of reduced temperature of chamber walls thus bringing the peak pressure closure to TDC. The peak pressures and rates of pressure rise are found to be higher for the insulated piston at this injection timing.

Finite Element Analysis for Piston Temperature Distribution

Finite element analysis using the ANSYS program was adopted for estimating the temperature distribution within the conventional

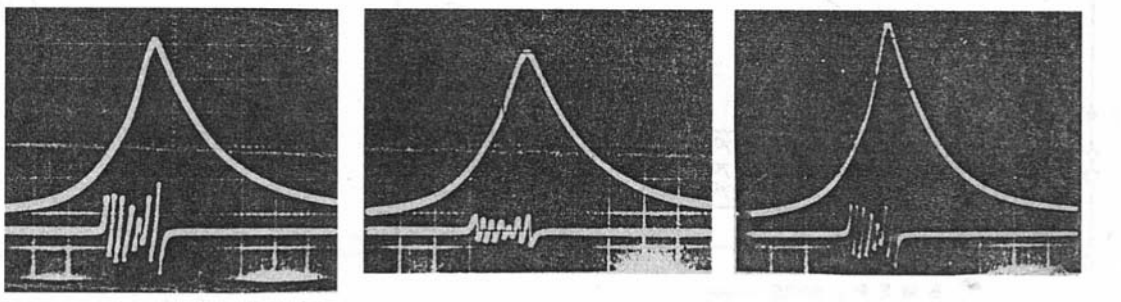

Fig. 10 Typical pressure-crank angle diagrams for conventional piston at 27° bTDC and insulated piston with Nimonic crown 27° bTDC and 29.5° bTDC

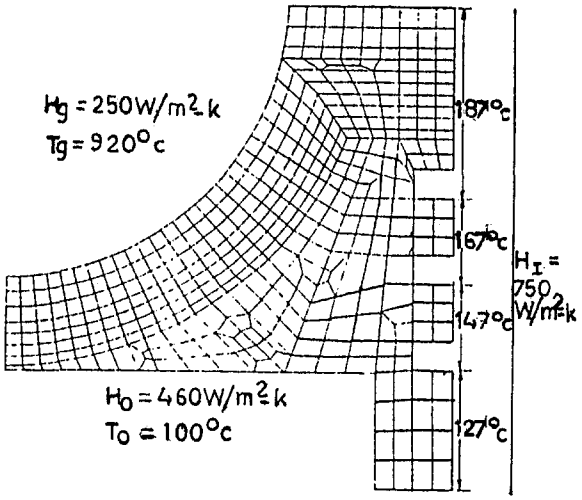

Fig. 12 Finite element mesh employed

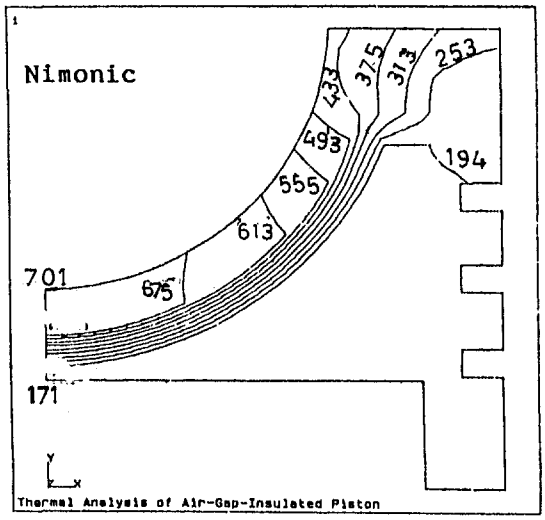

(*a*)

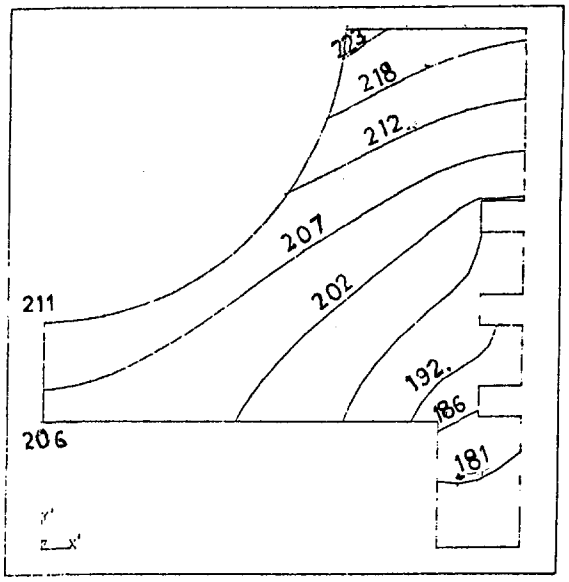

(*b*)

Fig. 13 (*a*) Isotherms in insulated piston with Nimonic crown having an air gap of 3 mm; and (*b*) isotherms in conventional piston

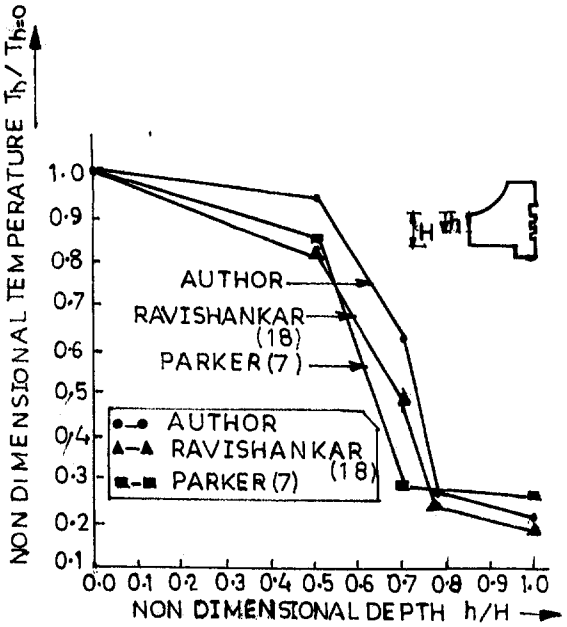

Fig. 14 Variation of nondimensional temperature with nondimensional depth with optimized insulated piston

and different configurations of the air gap insulated pistons. The mesh required for the analysis was generated using NISA software employing eight noded quadrilateral isoparametric elements. The heat transfer inside the air gap was considered to be by conduction only. Figure 12 shows the mesh generated for the present analysis along with the boundary conditions chosen (Rama Mohan et al., 1994).

Figures 13(*a*) and 13(*b*) show the distribution of isotherms in an insulated piston with an air gap of 3 mm and conventional piston, respectively. It is desirable that the temperatures and distances are nondimensionalized in order to show the trends instead of presenting the data in absolute magnitudes.

Figure 14 gives the nondimensional temperature variation along the axis of the piston with nondimensional depth for the insulated piston with Nimonic crown having 3 mm air gap, compared to the relevant data of other researchers (Parker and Donnison, 1987;

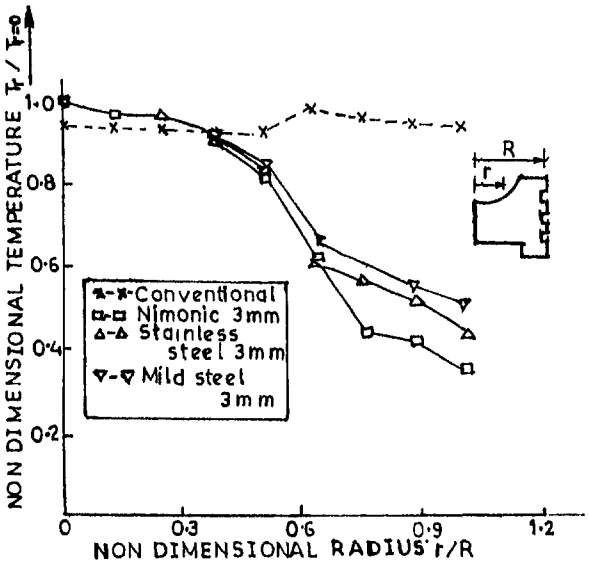

Fig. 15 Variation of nondimensional temperature with nondimensional radial distance for pistons with different crown materials having an air gap of 3 mm

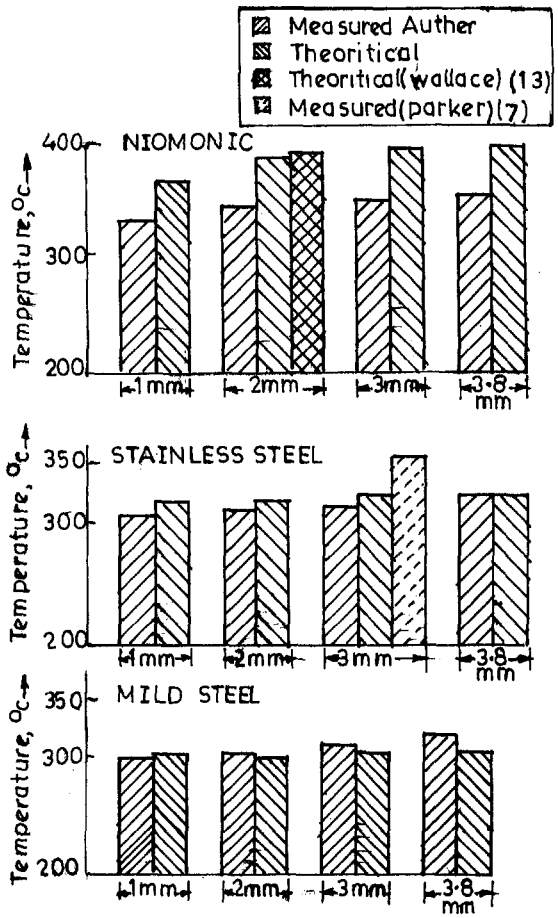

Fig. 16 Variation of air gap temperature with different air gap thicknesses obtained from theoretical and experimental evaluation

Ravishanker et al., 1989). The variation of nondimensionalized temperature with nondimensional radial distance is shown in Fig. 15 for a piston with a 3 mm air gap and different crown materials. While the temperature variation along the radial distance is negligibly small in the conventional piston due to the absence of thermal resistance, there is steep variation of temperature for an insulated piston.

Validation of the Computer Predicted Results

It is always necessary to validate the computer predictions by comparing to the results obtained from the experimental data or using the computations of the other researchers employing independent prediction techniques. Figure 16 shows the variation of air gap temperature with varying air gap thicknesses obtained theoretically and experimentally for the piston with the Nimonic crown.

The agreement between the trends of theoretical and measured values is reasonably good. However the theory predicted higher magnitudes of air gap temperatures over that of experimental results.

This is because experimental results take the average temperature of air in the air gap, while the computer predicts the average magnitudes taken from the upper and the lower isotherms of the air gap. Also, computer analysis neglected radiant and convective heat transfer effects in the air gap, so that higher magnitudes of air gap temperatures resulted. The above figure also presents the measured value of temperature in the air gap with the steel crown employed by Parker et al. (1987). The figure also gives the computer predicted values of air gap temperature estimated by Wallace et al. (1984) for a 2 mm air gap employing Nimonic crown. It is gratifying to note that the authors' results agreed exceedingly well with the data of the other researchers.

Analytical Predictions

A zero dimensional multi-zone combustion model was used to predict the performance of the low heat rejection diesel engine with air gap insulated piston. The model is a closed cycle simulation and has been divided into the following five sub models: (1) fuel injection; (2) spray penetration and air entrainment; (3) spray evaporation; (4) combustion model; and (5) heat transfer model.

Fuel Injection. The number of droplets and their Sauter mean diameter in each element are computed from the following relations (Glassman, 1977):

$$(D_{32})_{i,j} = [23.9(p_{inj} - p)^{-0.135}(\rho_a)^{0.12}]*(Q_{inj}) \quad (1)$$

$$N_{i,j} = \int_{t_i}^{t_{i+1}} Q_{inj}dt/(j*(\prod/6)(D_{32})^3_{i,j}). \quad (2)$$

Spray Penetration and Air Entrainment. The velocity of the element is found using the location of element X from the following relations (Glassman, 1977):

$$\text{for } t < t_b,$$

$$\frac{dX_{i,j}}{dt} = \frac{X_{i,j}}{t} \text{ for } j \geq 1. \quad (3)$$

The air entrainment into each element is obtained by momentum balance and is as shown below.

$$M_{aei,j} = M_{fi,j}\frac{\{V_{inj} - 1\}}{dX_{i,j}/dt} \quad (4)$$

The entrainment of the individual species into each element is given by

$$dM_{NS_{i,j}} = Y_{NS}\frac{\{dM_{aei,j}\}}{dt}. \quad (5)$$

Spray Evaporation. The evaporation rate of a droplet in an element is computed, using Spalding's droplet evaporation relation (Ravishanker, 1989) as

$$\frac{dM_f}{dt} = 4\prod r_s\rho_s D_s \log(1 + B) \quad (6)$$

The rate of decrease of droplet radius is shown by the following expression (Ravishanker, 1989):

$$\frac{dr_s}{dt} = [\rho_s D_s/(\rho_l r_s)] \log(1 + B) \quad (7)$$

Combustion Model. The ignition delay is obtained from,

$$\tau = 4*10^{-3}(p)^{-2.5}(phi)^{-1.04} \exp 4000/T. \quad (8)$$

The mass of air and mass of gaseous fuel determine equivalence ratio in the gaseous element is given by

$$phi = (M_{fg}/M_a)/(M_{fg}/M_a)_{st}. \quad (9)$$

Heat Transfer Model. Heat transfer to the cylinder walls is obtained using Annand's relation (Annand, 1963),

$$dQ_w/dt = aAk/D_l[F_w(\mathrm{Re})^b](T - T_w) + c(T^4 - T_w^4). \quad (10)$$

In the above equation, the total heat transfer surface is considered to be made up of different sub areas as shown below.

$$A = A_p + A_l + A_h \quad (11)$$

In Eq. (11), the wall temperature T has to be accurately employed based on experimental data. All the earlier researchers employed the surface temperatures of the piston, liner and

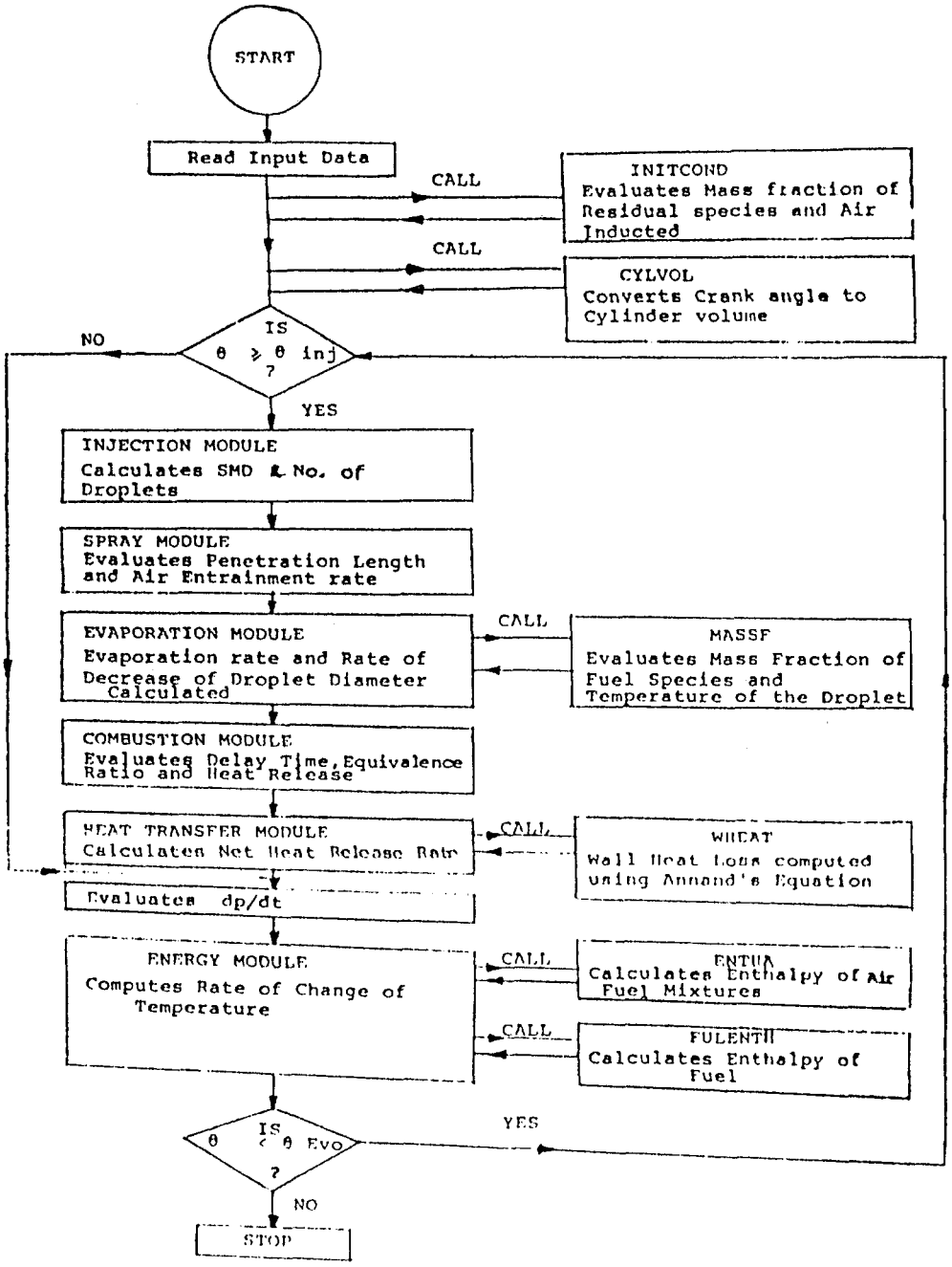

Fig. 17 Flow chart of computer model

cylinder head arbitrarily. In the present paper, though, the temperature of the liner and cylinder head are assumed to be constant, the piston temperature, however, is evaluated more accurately from the isotherms of the piston obtained using FEM analysis (Rama Mohan et al., 1994). The net heat release in an element is given by

$$\frac{dQ_{n_{i,j}}}{dt} = \frac{dQ_{c_{i,j}}}{dt} - \frac{dQ_{v_{i,j}}}{dt} - \frac{dQ_{w_{i,j}}}{dt},$$

where $dQ_{c_{i,j}}/dt$ is the heat release rate due to combustion and $dQ_{v_{i,j}}/dt$ is the rate of heat removal from the gas phase due to the latent heat of evaporation.

Pressure is obtained from conservation of momentum and is given by the following expression:

$$P = \left[\sum \frac{R}{C_{pij}} \{Q_n + M_{ae}(h_u - h_{ij}) - M_{ij}T_{ij}R_{ij} + M_v(h_i - h_{ij})\} + \sum M_{ij}T_{ij}R_{ij} + \sum R_{ij}T_{ij}M_{ij} - P(V - V_1) \right] \times \left[V - V_1 - \sum \frac{V_{ij}R_{ij}}{Cp_{ij}} \right].$$

The temperature of the element at any instant is obtained by applying the energy equation to each element and is given as

$$T = \frac{Q_n + VP + M_{ae}(h_a - h) + M_v(h_f - h)}{M(C_v + R)} - MTR/M(C_v + R).$$

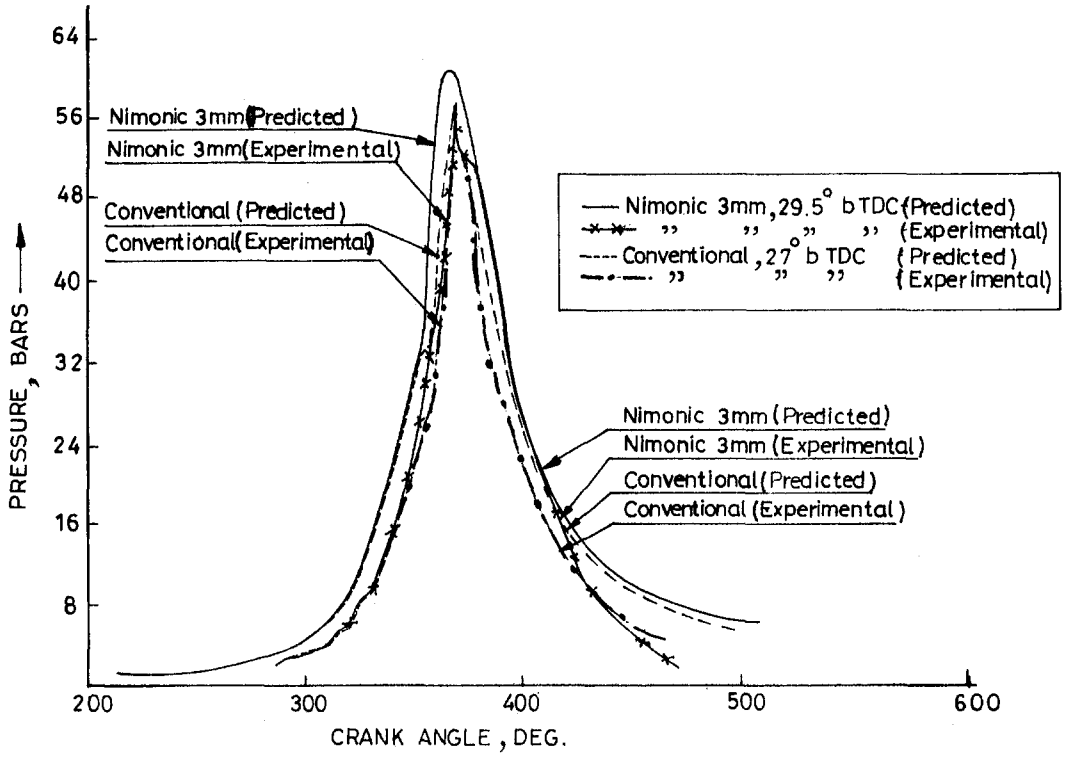

Fig. 18 Comparison to theoretical and experimental results of pressure crank angle data for the optimised piston engine and the conventional piston engine

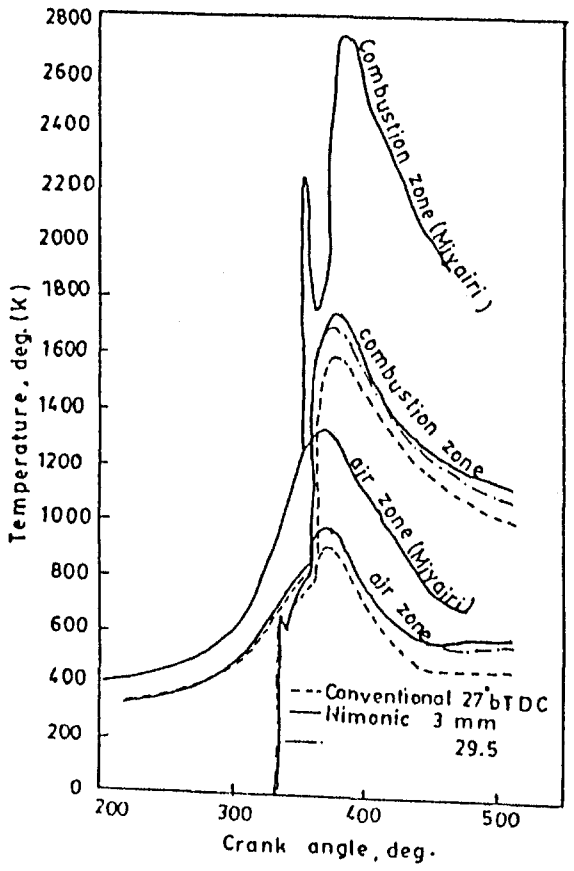

Fig. 19 Variation of temperature for conventional and optimized piston engine predicted from the combustion model

Solution Procedure

Equations (5), (6), (7), (13), and (14) form the set of governing equations which are solved using the Runge-Kutta fourth order scheme. A Fortran code has been prepared constituting the five submodels. A simplified flow chart of the computer program is shown in Fig. 17.

The heat loss to the coolant through the cylinder walls is estimated using Annand's equation (14), making use of more appropriate temperatures evaluated from the energy equation. Pressure is obtained from conservation of momentum. Figure 18 shows a comparison of the theoretical and the experimental results of pressure crank angle data for the cases of the optimized insulated piston with an injection timing of 29.5° bTDC and the conventional piston with an injection timing of 27° bTDC. The combustion model predicted higher values for both conventional and insulated piston engines in comparison with experimental results. The model also predicted higher magnitudes for the insulated piston in comparison with the conventional piston. It should also be observed that the predicted values were higher in comparison with the experimental data as the model assumes idealized combustion phenomenon.

The variation of gas and air temperatures with crank angle for the conventional piston engine with injection timing of 27° bTDC and the optimized piston engine with injection timing of 27 and 29.5° bTDC predicted from the analytical model are shown in Fig. 19. While the gas temperature has increased for the insulated engine in comparison with the 27° bTDC, there was a decrease of the gas for the insulated piston engine when the injection timing was advanced from 27° to 29.5° bTDC. The decrease in gas temperatures indicate saving of waste heat from exhaust while converting the same into useful work. This has been confirmed from the decreased BSFC observed with the advanced injection timings of the above insulated piston engine as seen from the Fig. 3. It is also observed that the insulated piston engine with an

injection timing of 29.5° bTDC still exhibits higher magnitudes over the conventional piston engine at 27° bTDC.

The above results provide excellent validation for the combustion model employed. For comparison purposes, the gas and air zone temperatures predicted by Miyairi on the basis of a two zone combustion model are also presented in figure. The two zone model being less realistic in comparison with the multi zone model, Miyairi predicted very high temperatures in the air and gas zones. However the trends agreed very well.

Conclusions

1 BSFC was reduced by 12 percent at part load and 4 percent at full load at an injection timing of 29.5° bTDC with the optimized insulated piston engine with a Nimonic crown and a 3 mm air gap in comparison with a conventional engine operating at an injection timing of 27° bTDC.
2 The heat rejection to the coolant for the optimized piston decreased by 12 percent in comparison with the conventional engine, while exhaust gas temperatures increased from 420°C to 435°C.
3 The smoke density for the optimized piston reduced throught the load range in comparison to the conventional piston. NOx and CO levels at full load increased marginally with optimized piston in comparison to the conventional piston.
4 Peak pressure and rates of pressure rise increased in the optimized insulated piston engine when the engine was operated at an injection timing of 29.5° bTDC.
5 Finite element analysis predicted an increase in the peak surface temperature from 225°C for the conventional piston to 703°C for the optimized piston. The temperatures measured with an L-link mechanism provided excellent validation for the FEM results.
6 Heat flow analysis showed a reduction of about 35.8 percent in heat flow through the optimized insulated piston in comparison with the conventional piston engine.
7 The multizone combustion model predicted pressure-crank angle data which agreed closely with experimental results obtained, the deviation in peak pressure being only 7 percent.

References

Alkidas, A. C., 1987, "Experiments With an Uncooled Single Cylinder Open Chamber Diesel," SAE Paper 870020.

Annand, W. D., 1963, "Heat Transfer in the Cylinder of Reciprocating Internal Combustion Engines," Proceedings, of I. Mech., Vol. 177 No. 36, pp. 970–990.

Cheng, W. K., Wong, V. W., and Gao, F., 1989, "Heat Transfer Measurements Comparison in Insulated and Noninsulated Diesel Engines," SAE Paper 890570.

Cole, R. M., and Alkidas, A. C., 1985, "Evaluation of an Air Gap Insulated Piston in a Divided Chamber Diesel Engine," SAE Paper 850359.

Glassman, I., 1977, *Combustion,* Academic Press, Inc., San Diego, CA.

Hiroyasu, H., 1980, "Simulation Program to Predict Direct Injection Diesel Engine Efficiency and Pollutant Emissions," research report, Dept. Mech. Engg., Hiroshima University.

Jabez Dhinagar, S., Siva Rama Prasad Rao, N., Nagalingam, B., and Gopal Krishnan, K. V., 1989, "Compensating the Volumetric Efficiency Drop of an Adiabatic Diesel Engine for Improved Performance," presented at the XI National Conference on I.C. Engines and Combustion, I. I. T., Madras.

Krishnan, D. B., Raman, N., Narayanaswamy, K., and Rohatgi, P. K., 1980, "Performance of Al-Si-Graphite Particle Composie Piston in a Diesel Engine," WEAR, Vol. 60 pp. 205–215.

Miyairi, Y., 1988, "Computer Simulation of an LHR Diesel Engine," SAE Paper 880187.

Miyairi, Y., Matsuhisa, T., Ozawa, T., Oikawa, H., and Nakashima, N., 1989, "Selective Heat Insulation of Combustion Chamber Walls for a DI Diesel Engine With Monolithic Ceramics," SAE Paper 890141.

Parker, D. A., and Donnison, G. M., 1987, "The Development of an Air Gap Insulated Piston," SAE Paper 870652.

Rafiqul Islam, M. D., Subramanyam, J. P., and Gajendra Babu, M. K., 1991, "A Thermodynamic Computer Simulation Model for a Low Heat Rejection Direct Injection Diesel Engine," presented at the X National Conference on I.C. Engines and Combustion, Rajkot, India.

Ravishanker, M. S., Seetharamu, K. N., Aswathanarayana, P. A., and Ramachandrarao, V. T. V. S., 1989, "FEM Analysis of Piston Insulation in an Adiabatic Engine," presented at the 11th National Conference on I.C. Engines and Combustion, I. I. T., Madras.

Rama Mohan, K., Rama Narayana, B. L., and Vara Prasad, C. M., 1994, "Computer Prediction of Temperature Distribution of an Air Gap Insulated Piston of an I.C. Engine by FEM Technique" presented at the IX National Convention on Computers in Mechanical Engineering, The Institution of Engineers, Hydevabad, India.

Siegla, D. C., and Alkidas, A. C., 1989, "Evaluation of the Potential of a Low Heat Rejection Diesel Engine to Meet Future EPA Heavy-Duty Emission Standards," SAE Paper 890291.

Wade, W. R., Havstad, P. H., Ounsted, E. J., Trinkler, F. H., and Garwin, I. J., 1984, "Fuel Economy Opportunities With an Uncooled DI Diesel Engine," SAE Paper 841286.

Wallace, F. J., Kao, T. K., Tarabad, M., Alexander, W. D., and Cole, A., 1984, "Thermally Insulated Diesel Engines," Proceedings, I. Mech. E., Vol. 198A, No. 5.

Woschni, G., Spindler, W., and Kolesa, K., 1987, "Heat Insulation of Combustion Chamber Walls—A Measure to Decrease the Fuel Consumption of I.C. Engines," SAE Paper 870339.